

Discovery of an Extended γ -ray Emission around the Supernova Remnant Candidate associated with PSR J0837–2454

PENGFEI ZHANG¹ AND YULIANG XIN²

¹*Department of Astronomy, School of Physics and Astronomy, Key Laboratory of Astroparticle Physics of Yunnan Province, Yunnan University, Kunming 650091, People's Republic of China; zhangpengfei@ynu.edu.cn*

²*School of Physical Science and Technology, Southwest Jiaotong University, Chengdu 610031, People's Republic of China; ylxin@swjtu.edu.cn*

ABSTRACT

Motivated by the recent discovery of a low surface brightness diffuse emission, a supernova remnant (SNR) candidate, surrounding the young pulsar PSR J0837–2454, we carry out a likelihood analysis of the γ -ray data obtained by the *Fermi* Gamma-ray Space Telescope from August 2008 to November 2022. Using a 2D Gaussian spatial template, we detect a significant extended γ -ray emission with a 68% containment radius of $\sim 1^\circ.8$, which is spatially coincident with the new SNR candidate at $\sim 12\sigma$ confidence level. The spectrum of the extended γ -ray emission, obtained in the energy range of 0.1–500.0 GeV, shows a significant spectral curvature at ~ 1 GeV, with a log-parabola spectral shape. Several scenarios, such as the SNR, pulsar wind nebula, and pulsar halo, are discussed as the potential origins of the extended γ -ray emission, and our model fitting results are preferred for the SNR scenario.

Keywords: Gamma-rays(637); Pulsars (1306); Supernova remnants (1667)

1. INTRODUCTION

During the ending stage of massive star evolution, the core of the star may undergo a powerful supernova explosion, collapsing into a rotating neutron star (i.e., a pulsar), which may lead to the creation of a supernova remnant (SNR), as the expanding gaseous remnant interacts with the surrounding circumstellar and interstellar medium. In our Galaxy, nearly 300 SNRs have been identified by the radio observations (Green 2014, 2019) at low Galactic latitudes $\lesssim 300$ pc (Maíz-Apellániz 2001). Thanks to the γ -ray telescopes, approximately 40 SNRs have been detected with γ -ray emissions (Zeng et al. 2019, and references therein), including the GeV γ -ray SNRs detected by *Fermi*, e.g. IC 443 and W44 (Ackermann et al. 2013), and the TeV γ -ray SNRs detected by the ground-based Cherenkov telescopes (e.g. HESS, HAWC, VERITAS and LHAASO), such as RX J1713.7–3946 (H. E. S. S. Collaboration et al. 2018a), G106.3+02.7 (Acciari et al. 2009; Albert et al. 2020; Cao et al. 2021), etc. SNR's electromagnetic emissions extend from MHz radio frequencies to TeV γ -ray energies (Zeng et al. 2019, 2021). The high-velocity shock of SNR could accelerate cosmic rays to very high energies (even up to hundred of TeV). The studies of the γ -ray emissions from SNRs provide us excellent tools for probing the interstellar medium and stellar evolution in our

Galaxy, especially for the Galactic cosmic rays acceleration.

Recently, Pol et al. (2021) reported a discovery and timing of a young pulsar PSR J0837–2454 at a high Galactic latitude with a Galactic coordinate (J2000) of $l = 247^\circ.6$ and $b = 9^\circ.8$. They presented the pulsar's timing solution by using the radio data from the Parkes radio telescope. Its spin period (P) and spin-down rate (\dot{P}) are 629.4 ms and 3.5×10^{-13} s s⁻¹, respectively. And the characteristic age ($\tau_c = \frac{P}{2\dot{P}}$; Lorimer & Kramer 2012) is 28.6 kyr based on the assumption that the magnetic-dipole braking as the only energy-loss mechanism with a braking index of 3 and $P \ll P_{\text{init}}$ (P_{init} is the pulsar's initial spin period). Its spin-down luminosity (\dot{E}) is calculated to be 5.5×10^{34} erg s⁻¹, and the surface dipole magnetic field strength (B_s) is 1.5×10^{13} G. Based on the NE2001 electron density model provided in Cordes & Lazio (2002), Pol et al. (2021) claimed that the pulsar locates at a larger distance of 6.3 kpc inferred by a DM-derived distances, which implies that PSR J0837–2454 appears at the edge of Galaxy and has a z-height above the Galactic plane of 1.1 kpc. If this value is true, PSR J0837–2454 will be the first pulsar known to be born from a runaway O/B star.

Furthermore, they also claimed a discovery of a low surface brightness diffuse emission with a region of \sim

$1^\circ.5$ extent concentrated around PSR J0837–2454 by using the archival Galactic and Extragalactic All-sky Murchison Widefield Array Survey (GLEAM; Hurley-Walker et al. 2017) data in 170–231 MHz bands¹. And the diffuse emission has a morphology consistent with a SNR. Based on the data from GLEAM and Southern H α Sky Survey Atlas (SHASSA; Gaustad et al. 2001), the distance for the diffuse emission is estimated to be ~ 0.9 and 0.2 kpc, respectively, which is much smaller than that predicted by Cordes & Lazio (2002). If the diffuse emission is indeed an SNR associated with the high Galactic latitude pulsar, searching for the multi-wavelength emission of the SNR, especially in γ -ray, would be helpful to study the particle acceleration and probe the interstellar medium above the Galactic plane. Motivated by their report, we carried out the data analysis with the γ -ray data surrounding PSR J0837–2454 collected by the Large Area Telescope onboard the *Fermi* Gamma-ray Space Telescope (*Fermi*-LAT; Atwood et al. 2009). And this paper is structured as follows: the likelihood analysis for the *Fermi*-LAT data and the main results are described in Section 2. Discussions of the probable physical origins for the extended γ -ray emission are shown in Section 3. In Section 4, we present a summary.

2. DATA ANALYSIS AND RESULTS

2.1. *Fermi*-LAT Data and source model

Around the position of PSR J0837–2454 reported by Pallanca et al. (2017) (R. A.= $129^\circ.49$, decl.= $-24^\circ.91$), there is a γ -ray point source named as 4FGL J0838.9–2502 in the Data Release 3 of the fourth *Fermi*-LAT source catalog (4FGL-DR3; Abdollahi et al. 2022) based on 12 yr data. In the 4FGL-DR3, 4FGL J0838.9–2502 has no associated source in other wavelengths, and its γ -ray spectrum is described by a log-parabola spectral shape (LP) of $dN/dE = N_0(E/E_b)^{-[\alpha+\beta \log(E/E_b)]}$ with $\alpha=2.60$, $\beta=0.45$ and $E_b=1.03$ GeV (Abdollahi et al. 2022). The following data analysis is aiming to determine the association between this γ -ray source and PSR J0837–2454 or the SNR around it.

Firstly, we carried out a whole data analysis in order to update the catalog’s parameters for the γ -ray sources in the region of interest (RoI) with the 14 yr *Fermi*-LAT observations. We selected the *Fermi*-LAT Pass 8 *Front+Back* events (evclass = 128 and evtype = 3) in the energy range of 0.1–500.0 GeV within a $20^\circ \times 20^\circ$ RoI centered at the position of 4FGL J0838.9–2502. The observations span from August 4 2008 to Novem-

ber 24 2022 (MJD: 54682.687–59907.214). The events with zenith angles $\geq 90^\circ$ were removed to exclude the γ -ray contamination from the Earth Limb. The expression of “DATA_QUAL > 0 && LAT_CONFIG == 1” was used, for *gtmktime*, to save the events having high-quality with flags of “good” in the good time intervals. In our data analysis, the instrumental response function of “P8R3_SOURCE_V3” and the software package of *Fermitools*–2.2.0 were used for the data reduction.

Based on the newest 4FGL-DR3 catalog, we used a python script, *make4FGLxml.py*², to create a model file. The model file includes all the spectral parameters of the γ -ray sources in 4FGL-DR3 within 25° around 4FGL J0838.9–2502. We freed the normalizations and spectral parameters for the sources within 5° of the ROI center, and the normalizations for the sources within 5° – 10° , together with the ones which are 10° outside but identified as variable sources. The normalizations of Galactic and extragalactic diffuse emission components were also set free. All other parameters in the model file were fixed to be their values provided in 4FGL-DR3. Then, a binned maximum likelihood analysis was performed between the whole LAT data set and the above model file. Then we saved all the best-fit parameters as a new model file. In order to reveal the γ -ray emissions around 4FGL J0838.9–2502, a TS map with a region of $6^\circ \times 6^\circ$ was created based on the new model with *gttsmap* by fixing all model parameters for all 4FGL-DR3 sources including the two diffuse backgrounds, and removing 4FGL J0838.9–250 from the model. The TS map is shown in the left panel of Figure 1, and a significant extended γ -ray emission (hereafter named as SG0837) is positional coincident with the SNR candidate reported in Pol et al. (2021).

2.2. Spatial Analysis

In order to study the spatial extension of the γ -ray emission from SG0837, we employed the *Fermi* ScienceTools packaged in Python (*Fermipy*) to derive the best-fit position based on the assumption that the SG0837 is a point source. Its coordinate was derived to be R. A.= $129^\circ.64$ and decl.= $-24^\circ.97$ with a 2σ error radius of $0^\circ.15$, which is shown as a purple cross in Figure 1, together with its error circle marked by the dashed circle. Based on the new coordinate, we obtained SG0837’s TS value to be ~ 82.44 as a point source. Then we used two spatial models, an uniform disk and a 2D Gaussian extended template, to describe the γ -ray emission from SG0837. The best-fit central positions and

¹ <https://vo.astron.nl/tgssadr/q.fits/cutout/form>

² <http://fermi.gsfc.nasa.gov/ssc/data/analysis/user/>

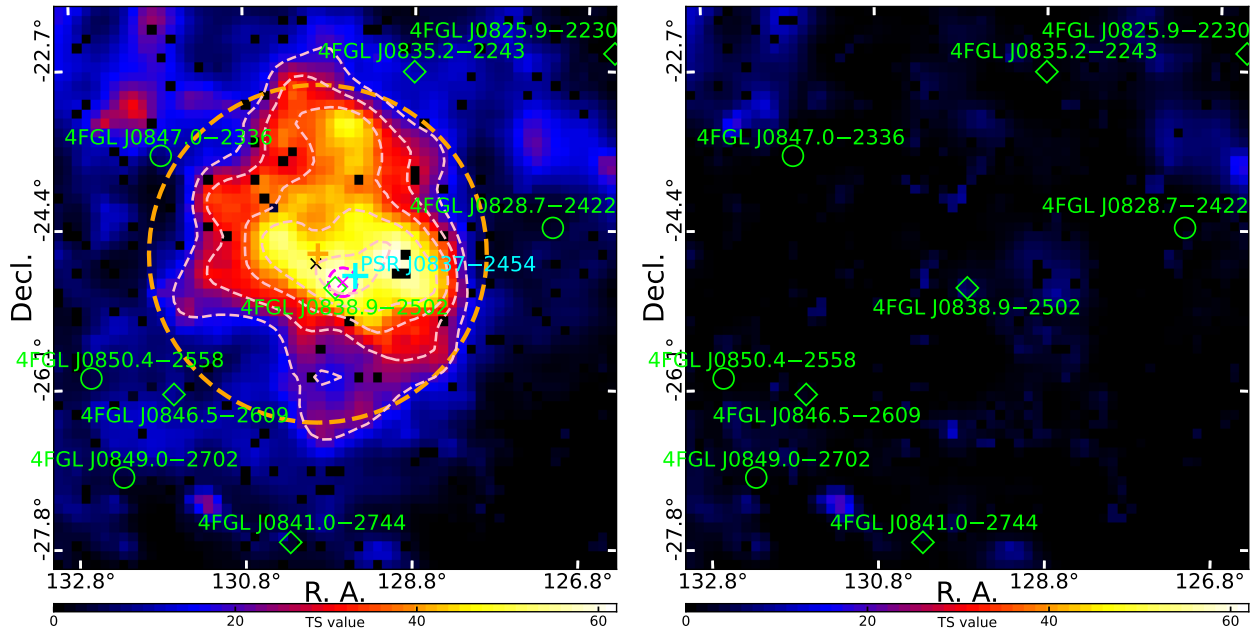


Figure 1. TS maps in 0.5–500.0 GeV covering $6^\circ \times 6^\circ$ region around the new found SG0837, centered at the position of 4FGL J0838.9–2502 with each pixel of $0^\circ.1$. Left panel: TS map for the γ -rays from SG0837. PSR J0837–24 is flagged with a cyan plus. The best-fit *Fermi*-LAT position of the 2D Gaussian template is marked with an orange plus, and its best-fit extension is indicated by an orange dashed circle. The best-fit positions of the uniform disk and point source models are marked with black and purple crosses, respectively. The positional uncertainty of point source is marked by the purple dashed circle. The pink contours are derived based on the TS value at each pixel, and the Δ TS between the neighbouring contours is 8.6. All γ -ray sources in the 4FGL are colored with green and labeled with ‘4FGL’. Right panel: the residual TS map by subtracting the γ -rays from all sources including SG0837. And the two TS maps share same scaled colorbar for convenient comparison.

Table 1. Spatial Analysis Results

Template ⁽¹⁾	Position ⁽²⁾	TS ⁽³⁾	Γ ⁽⁴⁾	$-\mathcal{L}$ ⁽⁵⁾	DoF ⁽⁶⁾
Point source	$129^\circ.64 \pm 0^\circ.06, -24^\circ.97 \pm 0^\circ.06$	82.44	2.54 ± 0.09	-1018839.61	4
Uniform disk	$129^\circ.95 \pm 0^\circ.09, -24^\circ.78 \pm 0^\circ.14; R_{68} = 1^\circ.97^{+0^\circ.25}_{-0^\circ.23}$	161.30	2.09 ± 0.05	-1018878.54	5
Uniform disk+Point source	—	158.98; 11.09	$2.07 \pm 0.09; 2.33 \pm 0.40$	-1018882.81	9
2D Gaussian	$129^\circ.93 \pm 0^\circ.14, -24^\circ.67 \pm 0^\circ.14; R_{68} = 1^\circ.80^{+0^\circ.25}_{-0^\circ.22}$	178.88	2.06 ± 0.04	-1018886.21	5
2D Gaussian+Point source	—	176.81; 9.81	$2.04 \pm 0.06; 2.34 \pm 0.29$	-1018890.01	9

Notes. Likelihood results of spatial analysis. (1) Spatial templates used in the spatial analysis. (2) Best-fit position and the radius containing 68% of the intensity (R_{68}) derived with package of *Fermipy*. The best-fit likelihood results of TS value, PL index, and $-\log(\text{Likelihood})$ values are listed in Columns (3), (4), and (5), respectively. (6) Degree of freedom (DoF) for source models.

extensions of the two extended templates are listed in Table 1.

Using the positions and extensions of the two spatial models, we performed the likelihood analysis again, and the best-fit results are summarized in Table 1. In these analysis, the spectral shape of power-law (PL), $dN/dE = N_0(E/E_0)^{-\Gamma}$, for each extended spatial model is employed in order to compare their likelihood results easily. The significance of the extension for a γ -ray source is defined by a likelihood-ratio test as shown in Lande et al. (2012), which can be calculated by $\text{TS}_{\text{ext}} = -2(\log \mathcal{L}_{\text{pt}} - \log \mathcal{L}_{\text{ext}})$, where \mathcal{L}_{pt} (null hypothesis)

and \mathcal{L}_{ext} (alternative hypothesis) are the maximum likelihood values for point source model and spatial extended source model, respectively. For the likelihood results listed in Table 1, we found that the 2D Gaussian template is significantly preferred to the point source model with $\text{TS}_{\text{ext}} \sim 93$, which corresponds to the significance level of 9.6σ with one additional degree of freedom (DoF).

The TS value of the 2D Gaussian template is 178.88 in the likelihood analysis based on the spectral shape of PL, corresponding to a significance level at $\sim 12\sigma$ with five DoFs. The best-fit position of the 2D Gaussian template

was derived to be R. A.=129°.93 and decl.=−24°.67 with a 68% containment radius of $\sim 1^\circ.8$. The position and extension are shown in Figure 1 with an orange plus and a dashed circle, respectively. From Figure 1, we can see that the angular radius visually encloses the most of extended γ -ray emissions from SG0837. We updated the model file with the best-fit values in this likelihood analysis with the 2D Gaussian template. Then a residual TS map was created based on the updated model by fixing all model parameters for all sources (including SG0837) in the model file, which is shown in the right panel of Figure 1. None of obvious excess suggests that 2D Gaussian template can well describe the SG0837’s γ -ray emission.

Meanwhile, we also tested other complex models, i.e. 2D Gaussian/uniform disk plus a point source, and the likelihood results are shown in Table 1. The TS of the point source is not significant with $TS_{PS} < 16$, and these models are not favored in the further analysis. Moreover, we also performed a timing analysis by folded the *Fermi*-LAT data using the ephemeris for PSR J0837–2454 (Pol et al. 2021), while no creditable pulsation was found. These analysis make PSR J0837–2454 to be a radio loud and γ -ray quiet pulsar.

2.3. Spectral Analysis

To test SG0837’s spectral properties in γ -rays, we used a spectral form of LP to fit the γ -rays from SG0837 in 0.1–500.0 GeV. And the corresponding TS_{LP} value of SG0837 is calculated to be ~ 198 . Other parameters α , β , and E_b are fitted to be 2.23 ± 0.22 , 0.29 ± 0.09 , and 1.4 ± 0.4 GeV, respectively. The corresponding integrated photon and energy fluxes are $(1.36 \pm 0.21) \times 10^{-8}$ photons $\text{cm}^{-2} \text{s}^{-1}$ and $(1.26 \pm 0.18) \times 10^{-11}$ erg $\text{cm}^{-2} \text{s}^{-1}$, respectively. The variation of TS value between LP and PL models is $\Delta TS = TS_{LP} - TS_{PL} \sim 19$, corresponding to a significance level of $\sim 4.4\sigma$. Hence we suggest that the LP model is relatively better to the PL one to describe the gamma-ray emission from SG0837.

Then we saved the best-fit parameters into a final model file, and fixed the spectral parameters for all the sources in the model file to be the above likelihood analysis values. The normalizations for the sources within 10° around the ROI center and the two diffuse backgrounds were left free. Based on the final model file, we extracted a spectral energy distribution (SED) for SG0837 in the energy range of 0.1–500.0 GeV by adopting the spatial template of the 2D Gaussian and the global spectral shape of LP. The data were divided into 12 equal logarithmically spaced energy bins, and the individual likelihood analysis was employed for each bin.

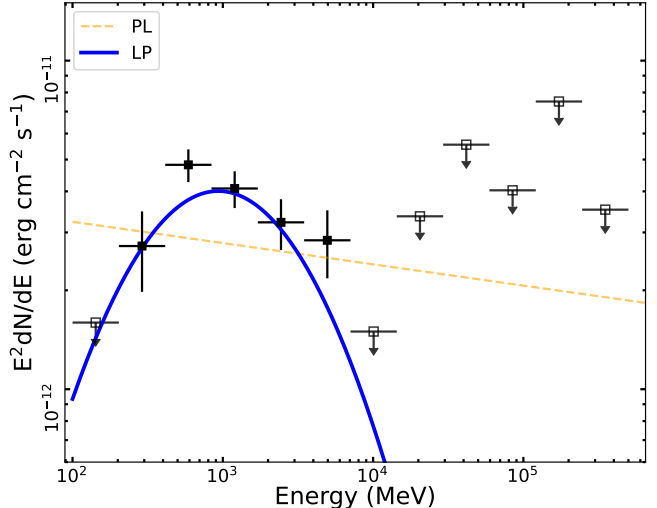


Figure 2. γ -ray SED of SG0837 obtained from the data in 0.1–500 GeV. The best-fit LP and PL spectral shapes are shown as the blue solid and yellow dashed lines, respectively. The flux data points with $TS > 10$ are shown with the black squares with the pluses as their uncertainties, and the black arrows indicate the 95% upper limits.

We show the γ -ray spectrum of SG0837 in Figure 2, in which the 95% flux upper limit is calculated for the energy bin with TS value of SG0837 lower than 10. The global fitting with LP and PL models are also plotted with the blue solid and yellow dashed lines, respectively. Comparing the best-fit LP and PL models in Figure 2, SG0837’s γ -ray SED in 0.1–500.0 GeV is relatively well described by the LP model, which is in agreement with the result shown by ΔTS .

3. POSSIBLE GAMMA-RAY ORIGINS

3.1. Supernova Remnant

According to the discovery in Pol et al. (2021), thus the origin of the SNR scenario for the γ -ray emission from SG0837 is considered. The γ -ray spectra of tens of *Fermi*-LAT observed SNRs can be basically divided into two classes (Zeng et al. 2019): one has the hard GeV γ -ray spectrum with the spectral curvature at $\sim \text{TeV}$, which corresponds to the young-aged SNR, like RX J1713.7-3946 (H. E. S. S. Collaboration et al. 2018a) or RX J0852.0-4622 (H. E. S. S. Collaboration et al. 2018b). And the γ -ray emissions from these SNRs are typically suggested to be from inverse Compton scattering (ICS) of accelerated electrons (leptonic process). Another class shows the spectral break at $\sim \text{GeV}$, which corresponds to the old-aged SNRs interacting with molecular clouds, like IC 443 and W44 (Ackermann et al. 2013). And such γ -ray emissions are suggested to be from the decay of neutral pions produced by the inelastic proton-proton collisions (hadronic pro-

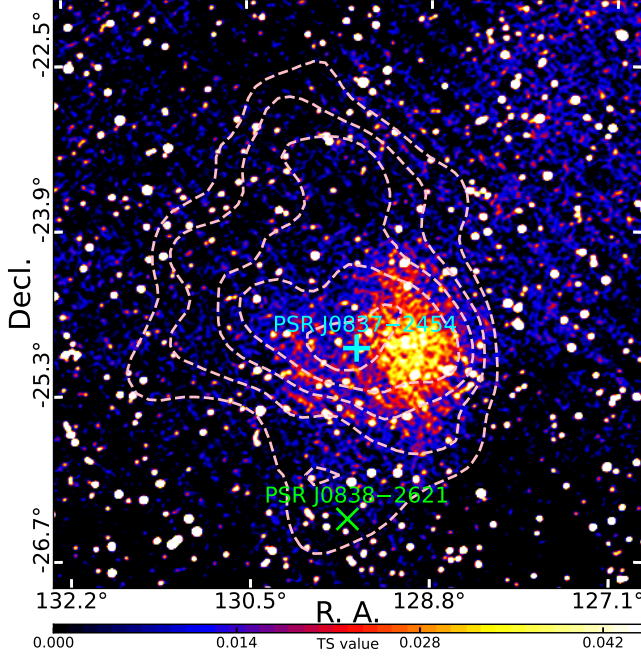


Figure 3. Radio imaging with a wide-field view around SG0837 in the stacked 170–231 MHz band data. The archival data are obtained from the TIFR GMRT sky survey, as reported in Figure 6 of Pol et al. (2021). PSR J0837–2454 is flagged with a plus, while the cross stands for the position of PSR J0838–2621 with a characteristic age of 1.3×10^5 kyr (Burgay et al. 2006). The pink contours show the GeV γ -ray emission of SG0837 drawn from Figure 1.

cess). The γ -ray spectrum of SG0837 is similar to that of IC 443 and W44, etc, and the hadronic model is also considered here for it. Considering the observational fact that the size of the γ -ray emission region is much larger than that of the remnant, which is shown as in Figure 3, the escaping scenario of protons is suggested, i.e. the γ -ray emission is produced by the protons accelerated and escaped from the shock of SNR, like the SNR W28 (Aharonian et al. 2008; Cui et al. 2018). Here we assume instantaneous injection of protons into an uniform emission zone at $T = 28.6$ kyr. Here the age of remnant is assumed to be the characteristic age of PSR J0837-2454 (Pol et al. 2021). The spectrum of injected protons is adopted to be a power-law with an exponential cutoff E_{cut} :

$$Q_{\text{inj}}(E) = Q_0 E^{-\Gamma} \exp(-E/E_{\text{cut}}). \quad (1)$$

Here the spectral index and cutoff energy of protons are adopted to be $\Gamma = 2.0$ and $E_{\text{cut}} = 3$ PeV, respectively. And the total energy of injected protons is assumed to be $W_{\text{p, inj}} = \eta E_{\text{SN}}$, where η is the fraction of the kinetic energy of SNR, E_{SN} , converted into the escaped proton energy, and the typical value of E_{SN} is adopted to be 10^{51} erg (Woosley & Janka 2005; Vink & Kuiper 2006).

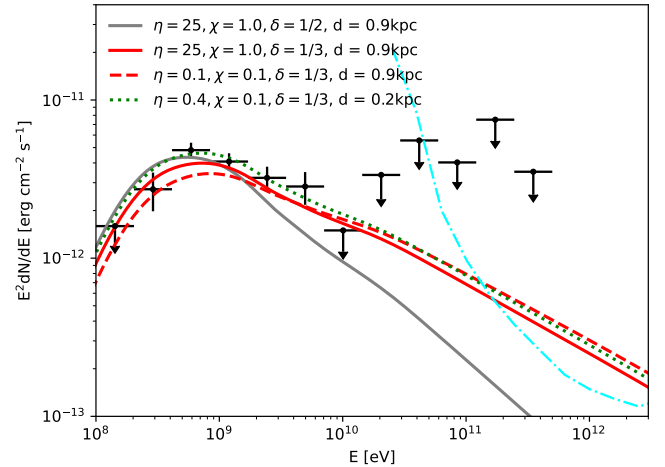


Figure 4. Modeling of the γ -ray spectra with the hadronic escaping model. The different lines indicate the scenarios with the different η , χ , δ and distance values as shown in the legend. The cyan dotted–dashed line shows the differential sensitivity of CTA-North (50 hrs; Cherenkov Telescope Array Consortium et al. 2019).

The proton spectrum within the emission region can be derived as Liu et al. (2020):

$$N_p(E, t) = \frac{Q(E)}{[4\pi D(E)T]^{\frac{3}{2}}} \int_0^R 4\pi r^2 dr \exp\left[-\frac{r^2}{4D(E)T}\right]. \quad (2)$$

And the diffusion coefficient of protons is assumed to be spatially consistent and energy dependent with $D(E) = \chi D_0 (E/E_0)^\delta$, where $D_0 = 3 \times 10^{28} \text{ cm}^2 \text{ s}^{-1}$ at $E_0 = 10$ GeV, and $\chi = 1.0$ corresponds to the typical value of Galactic diffusion coefficient (Blasi 2013). For an injected source spectrum given by $Q(E) \propto E^{-\Gamma}$ and $D(E) \propto E^\delta$, the spectrum of escaped protons, $N_p(E)$, approximately equal $Q(E)$ at low energies where the diffusion radius defined as $r_{\text{diff}} = \sqrt{4D(E)T}$ is much smaller than the size of the emission region R . Here R is adopted to be 28.3/6.3 pc with the distance of 0.9/0.2 kpc. And at high energies, $N_p(E)$ will follow $N_p(E) \propto E^{-(\Gamma + \frac{3}{2}\delta)}$, where the spectral break shown at $E_{\text{p, bre}}$ with $R = \sqrt{4D(E_{\text{p, bre}})T}$. With the different parameters of η , χ and δ adopted, the different spectra of escaped protons in the γ -ray emission region are produced and the corresponding γ -ray fluxes are calculated with the *naima* package (Zabalza 2015). And the value of the ambient gas density is assumed to be $n_{\text{gas}} = 1.0 \text{ cm}^{-3}$ considering the absence of the observations of molecular clouds in this region.

The resulting hadronic γ -ray flux with the different parameters are shown in Figure 4. Compared with the spectra of $\delta = 1/3$ with Kolmogorov turbulence for the

diffusion coefficient (Ptuskin et al. 2006), the higher value with $\delta = 1/2$ for Kraichnan turbulence gives a much softer γ -ray spectrum in the high energy, which is not very consistent with the observation. With the typical value of Galactic diffusion coefficient, $\chi = 1.0$, the total energy of injected protons is fitted to be 2.5×10^{51} erg, which is not reasonable. And the total energy of escaped protons above 1 GeV in this region is calculated to be $W_p = 1.5 \times 10^{49} (n_{\text{gas}}/1.0 \text{ cm}^{-3})^{-1}$ erg. It should be noted that the much higher total energies could be attributed to the underestimated of the gas density in this region. In addition, by fixing the total energy of injected protons to be 10^{50} erg, $\eta = 0.1$, the γ -ray spectrum with the distance of 0.9 kpc also can be explained by the hadronic escaping model with a lower diffusion coefficient, and such value is needed to be one order of magnitude lower than the typical Galactic value. And for the distance of 0.2 kpc, the total energy of injected protons need to be about 4×10^{50} erg with $\eta = 0.4$. And the corresponding total energy of escaped protons in the γ -ray emission region are estimated to be $W_p = 1.2 \times 10^{49} (n_{\text{gas}}/1.0 \text{ cm}^{-3})^{-1}$ erg and $W_p = 8.4 \times 10^{47} (n_{\text{gas}}/1.0 \text{ cm}^{-3})^{-1}$ erg for the distance of 0.9 kpc and 0.2 kpc, respectively.

3.2. Pulsar Wind Nebula

Taking into account the detected pulsar in the γ -ray emission region, a scenario of the pulsar wind nebula (PWN) driven by PSR J0837-2454 is also considered. Such extended γ -ray emissions are also detected in several typical PWNe, such as HESS J1825-137 (Principe et al. 2020), HESS J1640-645 (Xin et al. 2018), etc. However, these γ -ray PWNe detected by *Fermi*-LAT are driven by the energetic pulsars with spin-down powers between 10^{36} and 10^{39} erg s^{-1} (Acero et al. 2013). And the spin-down luminosity of PSR J0837-2454 with $\dot{E} = 5.5 \times 10^{34}$ erg s^{-1} seems to be too low to produce such energetic γ -ray emissions around it. So we suggest that the PWN scenario for the observed γ -ray emission for SG0837 is not favored.

3.3. Pulsar Halo

Along with the evolution of the PWN into the interstellar medium (ISM), the energetic particles could escape and their transport becomes to be dominated by diffusion. And these escaped particles could form a detectable halo around the pulsar, which is defined as a pulsar halo. Such halos are first detected as the extended TeV γ -ray emissions around the nearby low power pulsars Geminga and PSR B0656+14 (Abeysekara et al. 2017). And the searching for the GeV γ -ray emission for these pulsar halos is ongoing. While only the GeV

γ -ray emission from Geminga halo is detected by *Fermi*-LAT (Di Mauro et al. 2019), which is still under debate (Xi et al. 2019). Therefore, we also consider the possible origin as a pulsar halo for SG0837 around PSR J0837-2454 that detected here and discuss the potential TeV observation of it.

For the diffusion process in the pulsar halo, the diffusion size of particles is calculated as $r_d = 2\sqrt{Dt}$, and D represents the diffusion coefficient of particles. Considering the updated distance of 0.9 or 0.2 kpc for PSR J0837-2454 (Pol et al. 2021) and the 68% containment radius of $1^\circ.8$, the physical size of the γ -ray emission region is calculated to be 28.3 or 6.3 pc. Adopting the characteristic age of PSR J0837-2454 $\tau_c = 28.6$ kyr, the diffusion coefficient is estimated to be 2×10^{27} cm^2/s or 1×10^{26} cm^2/s for $d = 0.9$ or 0.2 kpc, respectively. And such values are much lower than the typical Galactic value of cosmic rays with $D \simeq 3 \times 10^{28}$ $\text{cm}^2 \text{ s}^{-1}$ (Blasi 2013).

Based on the definition of an electron halo in Giacinti et al. (2020), namely that of over-density of relativistic electrons around pulsar compared with the ISM, we calculated the energy density ϵ_e in relativistic particles around pulsar with established associated with the γ -ray emissions with $\epsilon_e = E_{\text{inj}}/V$, where V is the volume of the γ -ray emission region. And considering the non-detection of the TeV γ -ray emission from SG0837, the total injected energy is calculated based on the pulsar properties with $E_{\text{inj}} = \dot{E}\tau_c$, where \dot{E} and τ_c are the present spin-down power and characteristic age of the pulsar. For PSR J0837-2454, the energy density around is estimated to be 0.01 eV cm^{-3} or 1.0 eV cm^{-3} for the distance of $d = 0.9$ or 0.2 kpc. We replot the Figure 2 in Giacinti et al. (2020) by adding the values of PSR J0837-2454 in our Figure 5, together with PSR J0622+3749, which is identified to be a pulsar halo by LHAASO (Aharonian et al. 2021).

From Figure 5, we can see that the energy density around PSR J0837-2454 with $d = 0.2$ kpc and its current spin-down luminosity are close to the characteristics of TeV halo, like Geminga and PSR B0656+14. However, the characteristic age of PSR J0837-2454 is at least one order of magnitude lower than that of other halos. Hence, the extended γ -ray emission of SG0837 is not much favored for the halo scenario. Nonetheless, the potential TeV γ -ray emission from this source could be expected by the Cherenkov telescopes in the future.

4. SUMMARY

Pol et al. (2021) claimed a discovery and timing for a young pulsar PSR J0837-2454 with $P=629.4$ ms and $\dot{P}=3.5 \times 10^{-13}$ s s^{-1} by using the radio data from the

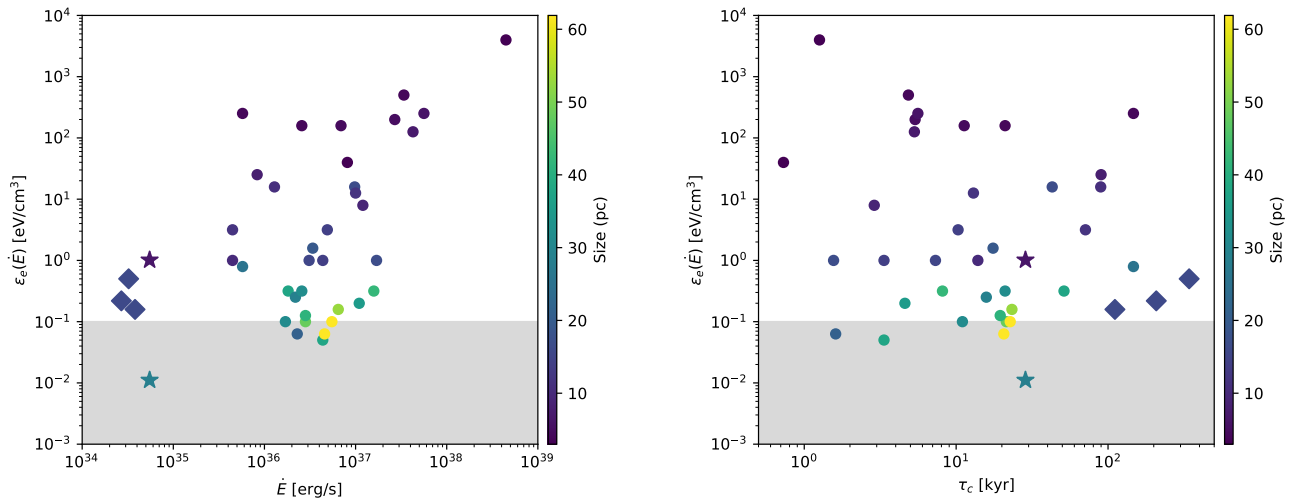


Figure 5. Energy density within TeV sources calculated as $\epsilon_e = \dot{E}\tau_c/V$ as a function of pulsar \dot{E} and τ_c following the Figure 2 in Giacinti et al. (2020) and the color bar shows the size of the γ -ray emission of each source. The shaded regions correspond to an energy density lower than that of the ISM of 0.1 eV cm^{-3} . The identified pulsar halos associated with Geminga, PSR B0656+14 (Abeysekara et al. 2017) and PSR J0622+3749 (Aharonian et al. 2021) are shown as the diamonds, and the stars represent PSR J0837–2454 with the different distances.

Parkes radio telescope. Moreover, an extended low-surface-brightness diffuse emission around PSR J0837–2454 was also detected by the radio data from the GLEAM, which suggests it to be a SNR candidate. Motivated by these, we analyzed the 14 yr γ -ray data from the *Fermi*-LAT observations surrounding PSR J0837–2454. Interestingly, we found a significant extended γ -ray emission named as SG0837 at a significance level of $\sim 12\sigma$ (see Figure 1), which is spatially coincident with the SNR candidate shown as in Figure 3. And SG0837 has a spatial extension with a 68% containment radius of $\sim 1^\circ.8$. The extension significance level is 9.6σ with a 2D Gaussian spatial model comparing with a point source model. And its SED in 0.1–500.0 GeV can be well described by the LP model.

PSR J0837–2454 is one of the relatively young pulsars compared with other cataloged pulsars. Pol et al. (2021) had shown 74 pulsars with characteristic age ≤ 28.6 kyr in their Figure 9 and summarised that 80% of 74 pulsars are often associated with a SNR and/or PWN. Considering the above percentage coupled with a diffuse emission in radio and an extended emission in γ -rays spatially coincident with the pulsar, we suggest that SG0837 is correlated with the SNR candidate around PSR J0837–2454. In our spatial analysis, no significant point source was found by subtracting the extended γ -ray emission from SG0837. And the γ -ray pulsation of PSR J0837–

2454 was also not found in the timing analysis. These factors make PSR J0837–2454 to be a radio loud and γ -ray quiet pulsar.

Several scenarios for the potential origins of the extended γ -ray emission are discussed, such as a SNR, PWN, or pulsar halo. Based on the model fitting results, see the discussion in Section 3, the γ -ray emission origin of the SG0837 is preferred for the SNR scenario. And the future potential detection in the TeV band by the Cherenkov Telescope Array in the northern hemisphere (CTA-North; Cherenkov Telescope Array Consortium et al. 2019) and the molecular clouds observations could be help to test the different models.

ACKNOWLEDGMENTS

We thank anonymous referee for her/his very helpful suggestions. This work is supported in part by the National Natural Science Foundation of China No. 12163006, No. 12233006 and No. 12103040, the Basic Research Program of Yunnan Province No. 202201AT070137, the joint foundation of Department of Science and Technology of Yunnan Province and Yunnan University No. 202201BF070001-020, and the Natural Science Foundation for Young Scholars of Sichuan Province, China (No. 2022NSFSC1808).

REFERENCES

Abdollahi, S., Acero, F., Baldini, L., et al. 2022, ApJS, 260, 53, doi: [10.3847/1538-4365/ac6751](https://doi.org/10.3847/1538-4365/ac6751)

Abeysekara, A. U., Albert, A., Alfaro, R., et al. 2017, Science, 358, 911, doi: [10.1126/science.aan4880](https://doi.org/10.1126/science.aan4880)

- Acciari, V. A., Aliu, E., Arlen, T., et al. 2009, *ApJL*, 703, L6, doi: [10.1088/0004-637X/703/1/L6](https://doi.org/10.1088/0004-637X/703/1/L6)
- Acero, F., Ackermann, M., Ajello, M., et al. 2013, *ApJ*, 773, 77, doi: [10.1088/0004-637X/773/1/77](https://doi.org/10.1088/0004-637X/773/1/77)
- Ackermann, M., Ajello, M., Allafort, A., et al. 2013, *Science*, 339, 807, doi: [10.1126/science.1231160](https://doi.org/10.1126/science.1231160)
- Aharonian, F., Akhperjanian, A. G., Bazer-Bachi, A. R., et al. 2008, *A&A*, 481, 401, doi: [10.1051/0004-6361:20077765](https://doi.org/10.1051/0004-6361:20077765)
- Aharonian, F., An, Q., Axikegu, Bai, L. X., et al. 2021, *PhRvL*, 126, 241103, doi: [10.1103/PhysRevLett.126.241103](https://doi.org/10.1103/PhysRevLett.126.241103)
- Albert, A., Alfaro, R., Alvarez, C., et al. 2020, *ApJL*, 896, L29, doi: [10.3847/2041-8213/ab96cc](https://doi.org/10.3847/2041-8213/ab96cc)
- Atwood, W. B., Abdo, A. A., Ackermann, M., et al. 2009, *ApJ*, 697, 1071, doi: [10.1088/0004-637X/697/2/1071](https://doi.org/10.1088/0004-637X/697/2/1071)
- Blasi, P. 2013, *A&A Rv*, 21, 70, doi: [10.1007/s00159-013-0070-7](https://doi.org/10.1007/s00159-013-0070-7)
- Burgay, M., Joshi, B. C., D’Amico, N., et al. 2006, *MNRAS*, 368, 283, doi: [10.1111/j.1365-2966.2006.10100.x](https://doi.org/10.1111/j.1365-2966.2006.10100.x)
- Cao, Z., Aharonian, F. A., An, Q., et al. 2021, *Nature*, 594, 33, doi: [10.1038/s41586-021-03498-z](https://doi.org/10.1038/s41586-021-03498-z)
- Cherenkov Telescope Array Consortium, Acharya, B. S., Agudo, I., et al. 2019, *Science with the Cherenkov Telescope Array*, doi: [10.1142/10986](https://doi.org/10.1142/10986)
- Cordes, J. M., & Lazio, T. J. W. 2002, *arXiv e-prints*, astro, doi: [10.48550/arXiv.astro-ph/0207156](https://doi.org/10.48550/arXiv.astro-ph/0207156)
- Cui, Y., Yeung, P. K. H., Tam, P. H. T., & Pühlhofer, G. 2018, *ApJ*, 860, 69, doi: [10.3847/1538-4357/aac37b](https://doi.org/10.3847/1538-4357/aac37b)
- Di Mauro, M., Manconi, S., & Donato, F. 2019, *PhRvD*, 100, 123015, doi: [10.1103/PhysRevD.100.123015](https://doi.org/10.1103/PhysRevD.100.123015)
- Gaustad, J. E., McCullough, P. R., Rosing, W., & Van Buren, D. 2001, *PASP*, 113, 1326, doi: [10.1086/323969](https://doi.org/10.1086/323969)
- Giacinti, G., Mitchell, A. M. W., López-Coto, R., et al. 2020, *A&A*, 636, A113, doi: [10.1051/0004-6361/201936505](https://doi.org/10.1051/0004-6361/201936505)
- Green, D. A. 2014, *Bulletin of the Astronomical Society of India*, 42, 47, doi: [10.48550/arXiv.1409.0637](https://doi.org/10.48550/arXiv.1409.0637)
- . 2019, *Journal of Astrophysics and Astronomy*, 40, 36, doi: [10.1007/s12036-019-9601-6](https://doi.org/10.1007/s12036-019-9601-6)
- H. E. S. S. Collaboration, Abdalla, H., Abramowski, A., et al. 2018a, *A&A*, 612, A6, doi: [10.1051/0004-6361/201629790](https://doi.org/10.1051/0004-6361/201629790)
- . 2018b, *A&A*, 612, A7, doi: [10.1051/0004-6361/201630002](https://doi.org/10.1051/0004-6361/201630002)
- Hurley-Walker, N., Callingham, J. R., Hancock, P. J., et al. 2017, *MNRAS*, 464, 1146, doi: [10.1093/mnras/stw2337](https://doi.org/10.1093/mnras/stw2337)
- Lande, J., Ackermann, M., Allafort, A., et al. 2012, *ApJ*, 756, 5, doi: [10.1088/0004-637X/756/1/5](https://doi.org/10.1088/0004-637X/756/1/5)
- Liu, S., Zeng, H., Xin, Y., & Zhu, H. 2020, *ApJL*, 897, L34, doi: [10.3847/2041-8213/ab9ff2](https://doi.org/10.3847/2041-8213/ab9ff2)
- Lorimer, D. R., & Kramer, M. 2012, *Handbook of Pulsar Astronomy*
- Maíz-Apellániz, J. 2001, *AJ*, 121, 2737, doi: [10.1086/320399](https://doi.org/10.1086/320399)
- Pallanca, C., Beccari, G., Ferraro, F. R., et al. 2017, *ApJ*, 845, 4, doi: [10.3847/1538-4357/aa7ca6](https://doi.org/10.3847/1538-4357/aa7ca6)
- Pol, N., Burke-Spolaor, S., Hurley-Walker, N., et al. 2021, *ApJ*, 911, 121, doi: [10.3847/1538-4357/abe70d](https://doi.org/10.3847/1538-4357/abe70d)
- Principe, G., Mitchell, A. M. W., Caroff, S., et al. 2020, *A&A*, 640, A76, doi: [10.1051/0004-6361/202038375](https://doi.org/10.1051/0004-6361/202038375)
- Ptuskin, V. S., Moskalenko, I. V., Jones, F. C., Strong, A. W., & Zirakashvili, V. N. 2006, *ApJ*, 642, 902, doi: [10.1086/501117](https://doi.org/10.1086/501117)
- Vink, J., & Kuiper, L. 2006, *MNRAS*, 370, L14, doi: [10.1111/j.1745-3933.2006.00178.x](https://doi.org/10.1111/j.1745-3933.2006.00178.x)
- Woosley, S., & Janka, T. 2005, *Nature Physics*, 1, 147, doi: [10.1038/nphys172](https://doi.org/10.1038/nphys172)
- Xi, S.-Q., Liu, R.-Y., Huang, Z.-Q., Fang, K., & Wang, X.-Y. 2019, *ApJ*, 878, 104, doi: [10.3847/1538-4357/ab20c9](https://doi.org/10.3847/1538-4357/ab20c9)
- Xin, Y.-L., Liao, N.-H., Guo, X.-L., et al. 2018, *ApJ*, 867, 55, doi: [10.3847/1538-4357/aae313](https://doi.org/10.3847/1538-4357/aae313)
- Zabalza, V. 2015, *Proc. of International Cosmic Ray Conference 2015*, 922
- Zeng, H., Xin, Y., & Liu, S. 2019, *ApJ*, 874, 50, doi: [10.3847/1538-4357/aaf392](https://doi.org/10.3847/1538-4357/aaf392)
- Zeng, H., Xin, Y., Zhang, S., & Liu, S. 2021, *ApJ*, 910, 78, doi: [10.3847/1538-4357/abe37e](https://doi.org/10.3847/1538-4357/abe37e)